journal of the mechanical behavior of biomedical materials 110 (2020) 103895

Contents lists available at ScienceDirect

Journal of the Mechanical Behavior of Biomedical Materials

journal homepage: http://www.elsevier.com/locate/jmbbm

Impact of superhydrophobicity on the fluid dynamics of a bileaflet mechanical heart valve

Hoda Hatoum [a], Sravanthi Vallabhuneni [b], Arun Kumar Kota [b], David L. Bark [c], Ketul C. Popat [c], Lakshmi Prasad Dasi [a,*]

[a] Department of Biomedical Engineering, Georgia Institute of Technology, Atlanta, GA, USA
[b] Department of Mechanical and Aerospace Engineering, North Carolina State University, Raleigh, NC, USA
[c] Department of Mechanical Engineering, Colorado State University, Fort Collins, CO, USA

ARTICLE INFO

Keywords:
Superhydrophobicity
Reynolds shear stress
Viscous shear stress
Blood damage
Turbulence

ABSTRACT

Objective: The objective of this study is to evaluate the impact of superhydrophobic coating on the hemodynamics and turbulence characteristics of a bileaflet mechanical valve in the context of evaluating blood damage potential.

Methods: Two 3D printed bileaflet mechanical valves were hemodynamically tested in a pulse duplicator under physiological pressure and flow conditions. The leaflets of one of the two valves were sprayed with a superhydrophobic coating. Particle Image Velocimetry was performed. Pressure gradients (PG), effective orifice areas (EOA), Reynolds shear stresses (RSS) and instantaneous viscous shear stresses (VSS) were calculated.

Results: (a) Without SH coating, the PG was found to be 14.53 ± 0.7 mmHg and EOA 1.44 ± 0.06 cm^2. With coating, the PG obtained was 15.21 ± 1.7 mmHg and EOA 1.39 ± 0.07 cm^2; (b) during peak systole, the magnitude of RSS with SH coating (110Pa) exceeded that obtained without SH coating (40 Pa) with higher probabilities to develop higher RSS in the immediate wake of the leaflet; (c) The magnitudes range of instantaneous VSS obtained with SH coating were slightly larger than those obtained without SH coating (7.0 Pa versus 5.0 Pa).

Conclusion: With Reynolds Shear Stresses and instantaneous Viscous Shear Stresses being correlated with platelet damage, SH coating did not lead to their decrease. While SH coating is known to improve surface properties such as reduced platelet or clot adhesion, the relaxation of the slip condition does not necessarily improve overall hemodynamic performance for the bileaflet mechanical valve design.

1. Introduction

Mechanical aortic valves are prosthetic valves that are still heavily used in young low-risk patients who are in need of valve replacement. While mechanical aortic valves are well known for their long-term durability, they are plagued by the life-long anti-coagulation regimen that accompanies them. This is due to the artificial surfaces where blood clots can stick and blood damage, expressed whether in platelet activation, thrombus formation or hemolysis, that is the result of the non-physiological flow downstream of these valves. Moreover, despite anti-coagulation, thromboembolism remains the most common complication associated with mechanical valves affecting around 0.2–5.7%. Blood damage with mechanical valves has been heavily studied. Hemolysis has been highlighted in several clinical studies (Dale and Myhre, 1978; Shapira et al., 2009). In addition, thrombus formation was well documented in many other clinical studies (Roudaut et al., 2007a; Sultan et al., 2019). Even though mechanical valve designs improved modestly since the past 50 years, the materials used to construct these valves remained the same (e.g. pyrolytic carbon and titanium) and thrombosis and hemolysis continue to be their major drawback (Rajput and Zeltser, 2019; Baudet et al., 1985; Chang et al., 2001).

Reducing if not mitigating the occurrence of valve thrombosis and hemolysis is an important objective for every blood-contacting device (Vongpatanasin et al., 1996). The interface between blood and the material is a factor that can help with thrombus formation (Bezuidenhout and Zilla, 2013; Horbett and Brash, 1987). Numerous material treatments have been developed to diminish this risk (Jaffer et al.,

* Corresponding author. Department of Biomedical Engineering, Georgia Institute of Technology, 387 Technology Circle NW, Atlanta, GA, 30313, USA.
E-mail address: lakshmi.dasi@gatech.edu (L.P. Dasi).

https://doi.org/10.1016/j.jmbbm.2020.103895
Received 8 July 2019; Received in revised form 13 May 2020; Accepted 30 May 2020
Available online 6 July 2020
1751-6161/

2015), such as modification of surfaces with Poly(ethylene oxide) (PEO), implementing albumin-coated surfaces and Pyrolytic carbon-coated surfaces among many. Although mechanical valves have the Pyrolytic carbon-coated surfaces, in-vivo studies still show thrombus-related complications particularly near the hinges.

Superhydrophobic (SH) surfaces, that are extremely repellent to water, may be promising with respect to minimizing the thrombotic risk associated with blood-material interactions. Khorasani et al. and Sun et al. showed that SH surfaces provided reductions in platelet adhesion (Khorasani and Mirzadeh, 2004; Sun et al., 2005). Interest in SH surfaces has been rising also because of their potential applications in friction-drag reduction (Voronov et al., 2008).

From a hemodynamic perspective, turbulence has been found to be detrimental to blood cells whether platelets or red blood cells (Stein and Sabbah, 1974). Reynolds shear stresses (RSS) are adopted as a surrogate indicator of blood damage. The higher the RSS up to a certain threshold – despite not being well determined – the higher the likelihood of blood damage (Hatoum and Dasi, 2019; Hatoum et al., 2019). Several publications raised the concern that RSS may not be reflective of the physical environment of the cells as they are statistically computed, and suggested the addition of instantaneous viscous shear stresses for a complete and comprehensive blood damage evaluation (Ge et al., 2008).

A study by Bark et al. utilizing a SH spray on the leaflets of a mechanical valve showed a dramatic reduction in cell adhesion when placed into contact with blood, indicating a reduction in thrombotic potential caused by blood-material interactions (Bark et al., 2017). However, the turbulent characteristics in that study were not assessed. The objective of this study is to evaluate the impact of superhydrophobic coating application on the induced hemodynamics and turbulence characteristics of a bileaflet mechanical valve in the context of evaluating blood damage potential.

2. Methods

2.1. Superhydrophobic coating application on the mechanical valve leaflets

The valves used in this study were manufactured using high-resolution stereolithography as explained in a previous work (Hatoum and Dasi, 2019) and as shown in Fig. 1. The leaflets were 3D printed using the high resolution Stratasys Objet 30 Pro Desktop 3D Printer (Edina, Minnesota). The material utilized was VeroClear rigid transparent material. The SH coating used in this study is the commercially available spray coating Rust-Oleum NeverWet Clear Spray. The kit contains two pressurized cans, one for a bottom-coating layer and another for a top-coating layer. The coating layers of the spray were applied on both sides of the 3D printed leaflets of the 23 mm mechanical valve. The bottom coating was applied first, left to dry for 30 min then the top coat was applied and left to dry for 30 min as well.

The surface morphology, coating thickness and surface roughness (Fig. 2) were characterized using a Scanning Electron Microscope (SEM) and surface profilometry. From the SEM images, the average feature size is found to be ~35 nm and the average coating thickness ~13 μm for the SH coating. From the surface topography profile, the average surface roughness is ~10 ± 0.7 μm for the SH coating. The thickness of the mechanical heart valve leaflet is > 1 mm and the thickness of the SH coating is ~13 μm (i.e., ~1% of the valve thickness or less). Therefore, the effect of the SH coating on the bulk properties of the heart valve is insignificant.

2.2. Repeatability of coating

In this work, we fabricated superhydrophobic (SH) surfaces by placing the substrate at a distance of about 20 cm from the NeverWet spray nozzle and using about 8–10 sprays, until the surface is visually covered with the coating. For each NeverWet-based SH surface prepared, the advancing contact angle, receding contact angle and sliding angle of water are consistently 160 ± 3, 154 ± 3 and 2 ± 1°, respectively.

2.3. Hemodynamic assessment

The valve with and without SH coating was evaluated hemodynamically in a pulse duplicator under physiological conditions. The pulse duplicator is a left heart simulator (Fig. 3) composed of a fluid reservoir, a valve located between the reservoir and the pump to prevent backflow from occurring (playing the role of a mitral valve), a pump that is controlled by a compressor controlled by a LabVIEW program, a flow probe to measure the flow rate connected to a flow meter, a customized aortic valve chamber where the valves are tested, a compliance chamber downstream the aortic valve to simulate arterial compliance, and a resistance valve to control the flow. The aortic flow rate was measured with an ultrasonic flow probe (Transonic Inc., Ithaca, NY) and pressures were measured just upstream and downstream of the valve using

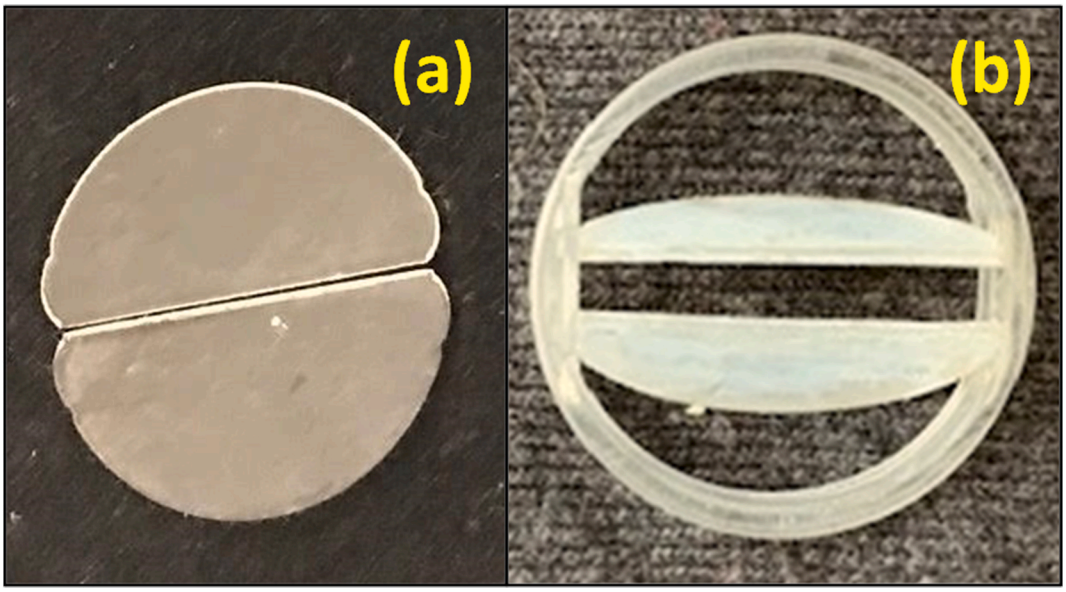

Fig. 1. Image of the valves utilized in the experiment: (a) 3D printed leaflets and (b) valve with mounted leaflets.

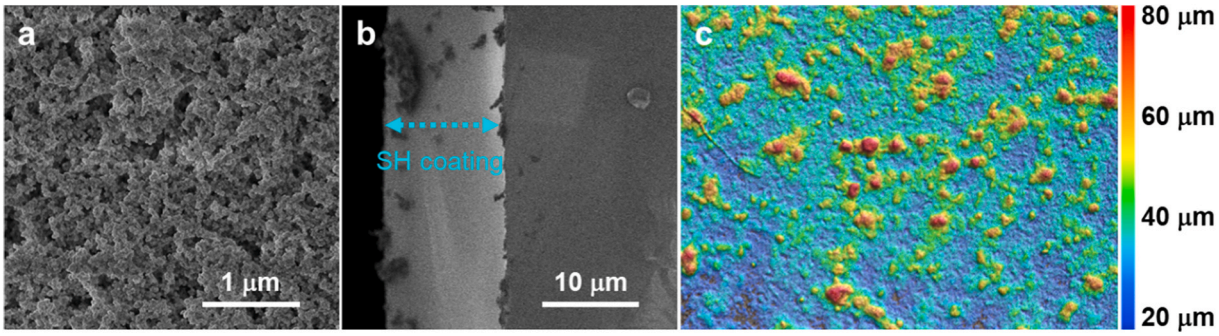

Fig. 2. (a) SEM image showing the morphology of the SH coating. (b) SEM image showing the thickness of SH coating. (c) Surface topography profile of the SH coating over a ~2.75 mm × 2 mm area.

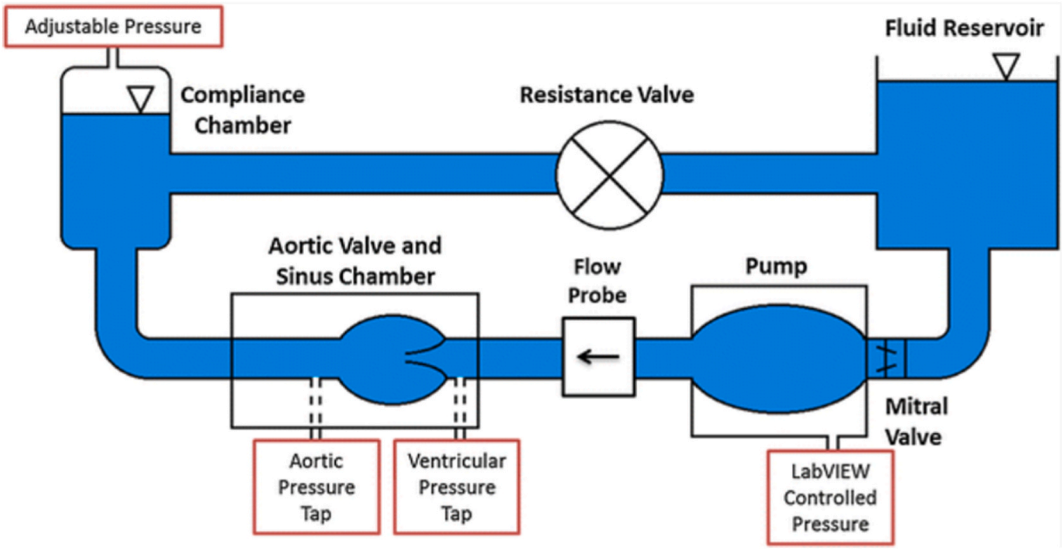

Fig. 3. Schematic of the pulse duplicating left heart simulator flow loop.

Validyne pressure sensors (Validyne Engineering Corp., Northridge, CA). More information on the flow setup can be found in previous publications (Hatoum and Dasi, 2019; Hatoum et al., 2019, Hatoum et al., 2019, 2019c, 2020).

The cardiac output chosen was 5L/min, heart rate was 60 beats per minute and pressures of 120/80 mmHg. The working blood analogue in this study was a mixture of water and glycerin with a density of 1060Kg/m^3 and viscosity of 3.5 cSt. A hundred consecutive cardiac cycles of flow and pressure were recorded at a sampling rate of 100 Hz. The transvalvular pressure difference – also known as pressure gradient (PG) clinically – is calculated as the difference between ventricular and aortic pressure.

The effective orifice area (EOA) is calculated based on the Gorlin equation:

$$EOA = \frac{Q}{51.6\sqrt{PG}} \tag{1}$$

where EOA is in cm2 (Shapira et al., 2009), Q is the root mean square of the flow in cm3/s (Roudaut et al., 2007a)/s over the same averaging interval of the PG (Pa).

2.4. Particle image velocimetry (PIV)

For particle image velocimetry, the fluid is seeded with fluorescent PMMA-Rhodamine B particles with average diameter of ~10 μm. These particles fluoresce once the region of the flow is illuminated with the laser beam and high-speed images were acquired. This involved illuminating the flow region using a laser sheet created by pulsed Nd:YLF single cavity diode pumped solid state laser coupled with external spherical and cylindrical lenses while acquiring high-speed images of the fluorescent particles within the region. In particular, the laser was generated using the Photonics Industries DM40-527 diode-pump Q-switched laser (Photonics, Bohemia, NY) with optics to covert the output beam into an expanded laser sheet. The laser had an initial thickness of approximately 1 mm, which was focused down to less than 200 μm within the measurement region using a spherical lens (f = 1 m).

The plane of measurement was aligned along the center plane of the chamber and was perpendicular to the leaflet axis. Fig. 4 shows the PIV plane orientation with respect to the valve.

Time-resolved PIV images were acquired with spatial and temporal resolutions of 0.0296 mm/pixel and 500 Hz respectively. 250 phase-locked measurements were recorded at acceleration, peak and deceleration with a spatial resolution of 0.0296 mm/pixel. The velocity resolution is 0.2368 mm based on a 16 × 16 interrogation window with 50% overlap. Velocity vectors were calculated using adaptive cross-correlation algorithms. Vorticity was calculated as follows:

$$\omega_z = \frac{dV}{dx} - \frac{dU}{dy} \tag{2}$$

with U and V being the x and y components of the velocity. The x and y directions are axial and lateral respectively with the z direction being out of plane measurement.

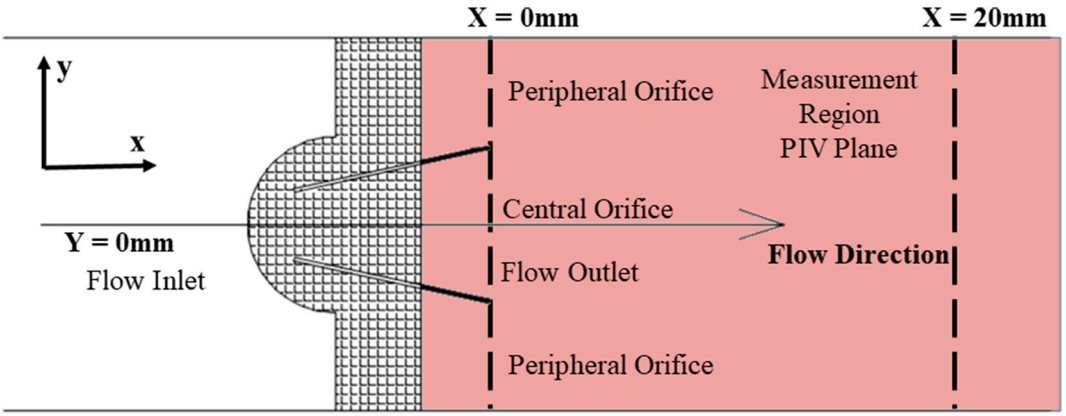

Fig. 4. Schematic of the flow through the bileaflet mechanical valve along with the measurement and PIV plane.

The viscous shear stress (VSS) was calculated as follows:

$$\tau = \mu\left(\frac{dU}{dy} + \frac{dV}{dx}\right) \tag{3}$$

where τ is in Pa and μ is the dynamic viscosity in N.s/m.

Because blood damage has been correlated to elevated turbulence in literature (Kameneva et al., 2004; Grigioni et al., 1999), and because Reynolds shear stresses (RSS) constitute an indicator on the turbulence level, they are computed in this study. The maximum RSS obtained from the RSS tensor was computed as follows:

$$RSS = \rho\sqrt{\left(\frac{\overline{u'u'} - \overline{v'v'}}{2}\right)^2 + (\overline{u'v'})^2} \tag{4}$$

where ρ is the blood density and u' and v' are the instantaneous velocity fluctuations in the x and y directions respectively. RSS is in Pa.

Turbulent kinetic energy (TKE) is a measurement of the kinetic energy of eddies and indicates turbulence intensity (Gunning et al., 2014).

$$TKE = \frac{1}{2}\left(\overline{u'^2} + \overline{v'^2}\right) \tag{5}$$

2.5. Error considerations

The sources of error in the PIV measurements are due to resolution as well as random error. Random errors are addressed in this study through statistical averaging of repeated measurements and statistical comparisons. This section briefly outlines the errors in accuracy due to limited resolution of the measurement techniques at hand. The conservative error estimate in velocity is <2% (i.e. particle displacements may be off by ±0.2 pixels out of total displacement of 10 pixels). Laser pulse timing errors are negligible in comparison. Now, given that the laser pulse separation was 0.30 ms, and the spatial resolution was at 29.6 μm, we estimate that instantaneous shear stress measurements are accurate to <0.16 Pa. The instantaneous shear stress bursts were as high as ~8 Pa. Thus, the large burst of shear stress that a particle in the turbulent jet may experience is accurate to within 2%. The independent repeats and statistical analysis further provide a solid basis to judge the reliability of our measurements.

3. Results

3.1. Hemodynamic parameters

Without coating, the PG was found to be 14.53 ± 0.7 mmHg and EOA 1.44 ± 0.06 cm^2. With coating, the PG obtained was 15.21 ± 1.7 mmHg and EOA 1.39 ± 0.07 cm^2.

3.2. Velocity field

Fig. 5 shows the instantaneous vorticity contours and velocity vectors at different phases during the cardiac cycle for the two valves with and without superhydrophobic coating. Though not drastically different, the vorticity structures in the wake of the leaflets with SH coating seem to be characterized by more intense vorticity, and vortex shedding and more mixing in the distal flow field. Fig. 6 shows the phase averaged velocity vectors and vorticity contours at acceleration, peak and deceleration for the valves with and without SH coating. Higher vorticity is present in the shear layers of the valve with SH coating during all phases. Thinner shear layers are noted with the SH coated valve compared with the valve without SH coating along with a slower decay of the middle and peripheral orifice ones until the end of deceleration. Without SH coating, faster dissipation is noted in the middle jet compared to the peripheral ones. With SH coating, there were no differences in dissipation rates between the middle and the peripheral jets shear layers.

Fig. 7 shows the normalized velocity profiles by the maximum of each curve versus x and y. In Fig. 7a, during peak systole without SH coating, the velocity is higher at the peripheral jets compared to the middle one and with the SH coating the velocity at the middle jet was higher than that measured at the peripheries. During peak, Fig. 7b shows the normalized velocity change versus x of the valves. There exists a faster decay with the SH coated valve compared to the valve without any coating. At the end of the measurement zone, the velocity reached 79.2% of the highest magnitude with the valve without coating while it reached 59.1% of the highest magnitude with the SH coated valve. To get a broader idea about how velocities in x and y directions are distributed downstream of the valves in the shear layer area, the probability density distribution of the instantaneous velocities during the cardiac cycle is plotted in Fig. 8. The limits of the areas are shown in the inset of the figure. More U range is obtained with SH coating compared to without in upper and lower shear layers and consequently in the complete combination of both shear layers (reaching almost 1.55m/s compared with 1.40m/s). Also, higher Vy are obtained with SH coating valve, in addition to higher oscillations between negative and positive values, going from −1.0Pa to +1.0Pa whereas those obtained without SH coating oscillate between −0.5Pa and +0.75Pa.

3.3. Turbulence results

Fig. 9 shows the principal Reynolds shear stress (RSS) contours during acceleration, peak and deceleration of both valves. Higher RSS are found with the SH coated valve downstream the leaflets compared to the valve without any coating during acceleration. The peak RSS are also distributed differently downstream the valves. To quantify RSS further, Fig. 10 shows the probability distribution of RSS magnitudes over the

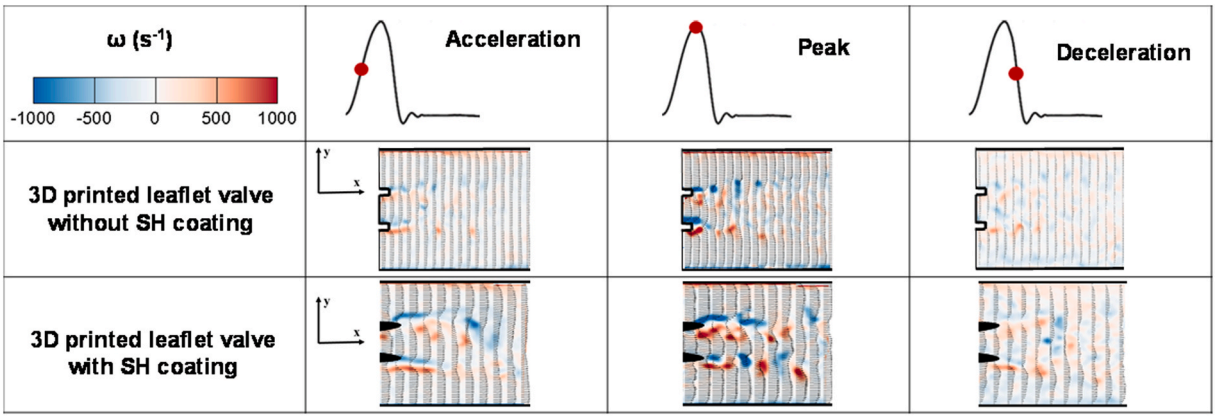

Fig. 5. Instantaneous vorticity contours and velocity vectors at different phases during the cardiac cycle for the two valves with and without super-hydrophobic coating.

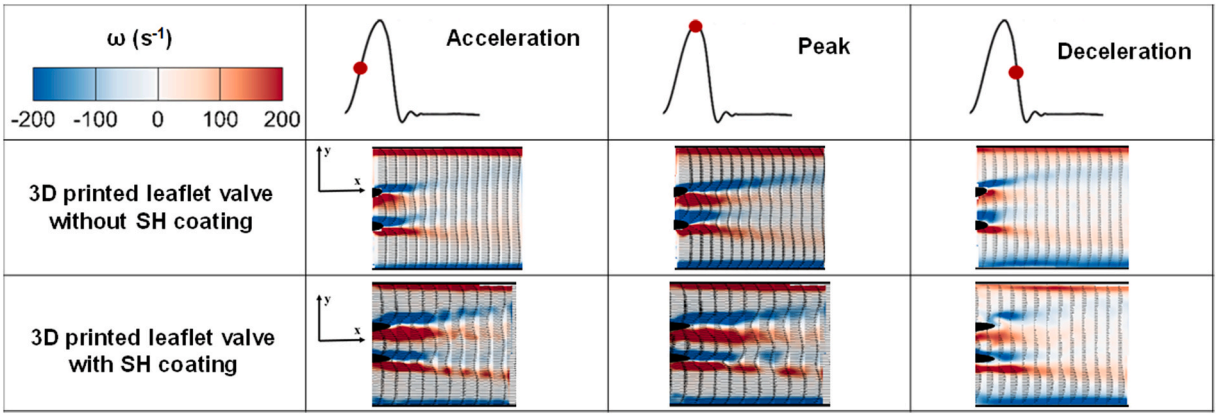

Fig. 6. Phase averaged velocity vectors and vorticity contours at three different phases in the cardiac cycle for the valves with and without SH coating.

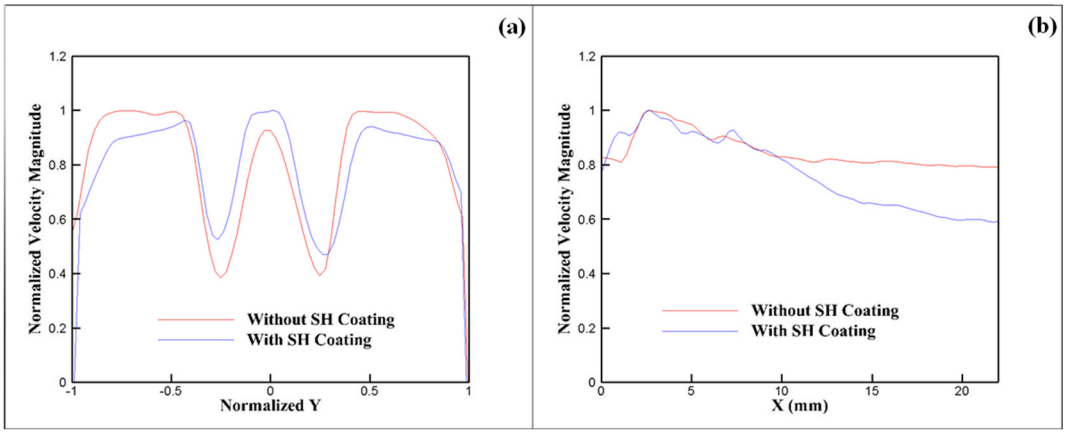

Fig. 7. Normalized averaged velocity profiles (by the maximum of each individual curve) right after the leaflets are open (X = 0) versus (a) normalized y and (b) versus x during peak systole.

region downstream of the valve. From this figure, during acceleration (**10a**), the RSS magnitudes with SH coating were 4 times larger than those obtained without SH coating (~20 Pa versus ~80Pa). In Fig. 10b during peak, the magnitude of RSS with coating (110Pa) exceeded that obtained without SH coating (40 Pa). In addition, the probability to develop higher RSS magnitudes were larger than those without SH coating at this phase. During deceleration (Fig. 10c), the RSS range with SH coating was found to be higher than that obtained downstream of the valve without any coating (16 Pa versus 9.9 Pa).

To connect the results above with the fluctuating components of velocity, Fig. 11 shows the standard deviation contour plots of the random velocity fluctuations U′ and V′ for the valve models at peak systole without and with SH coating. Significantly higher fluctuations are obtained with SH coating compared to without any SH coating in both directions x and y. The contour plots show not only higher magnitudes but also a persistent plot of elevated velocity fluctuation magnitudes downstream of the valve leaflets with SH coating compared to a more localized high fluctuation area without SH coating.

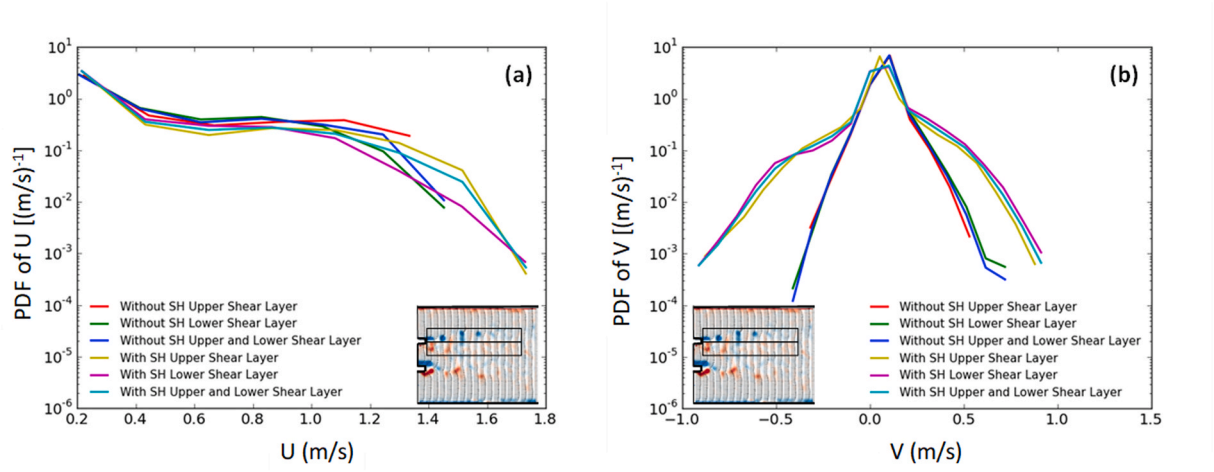

Fig. 8. Probability distribution of instantaneous velocity magnitudes in the x direction (a) and the signed velocity component in the y direction (b) of the valves with and without SH coating throughout the cardiac cycle.

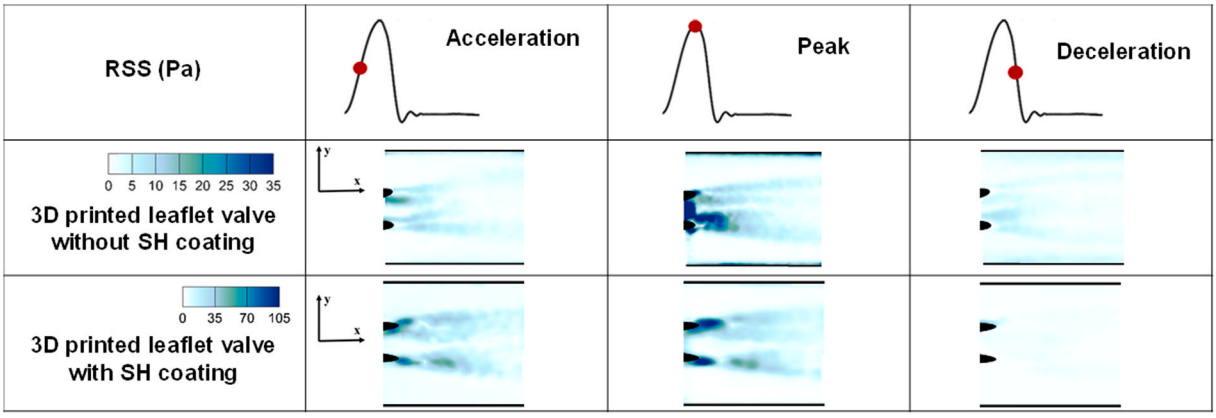

Fig. 9. Reynolds shear stress contours of the different valve cases at different time point throughout the cardiac cycle.

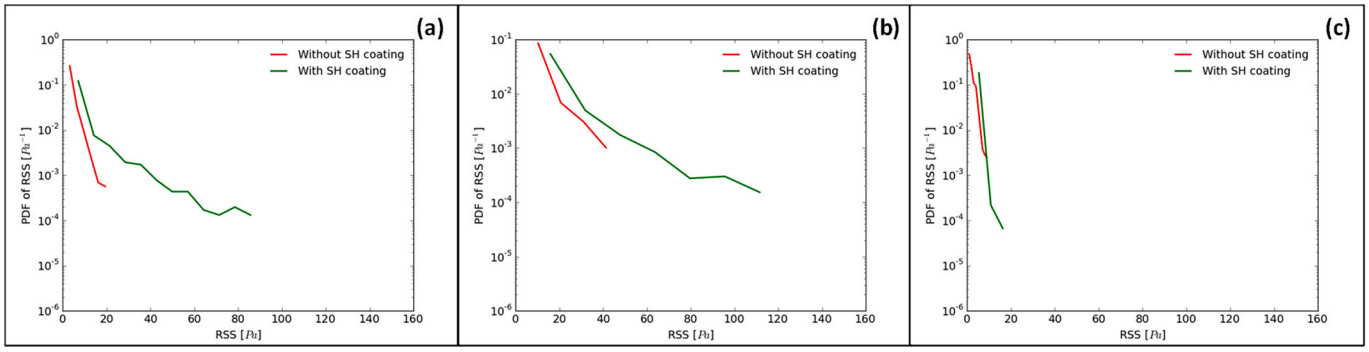

Fig. 10. Probability distribution of Reynolds shear stress magnitudes of the valves with and without SH coating at (a) acceleration, (b) peak and (c) deceleration.

In terms of turbulent kinetic energy, Fig. 12 shows TKE contours. As previously noted with the RSS contours, higher TKE magnitudes are obtained with SH coating compared to without coating obvious specifically during acceleration. During peak systole and deceleration, the maximal magnitudes were almost same reaching up to 0.162 m^2/s^2.

3.4. Instantaneous viscous shear stress results

Fig. 13 shows the instantaneous viscous shear stress contours at different phases during the cardiac cycle for the two valves. Similar to the instantaneous vorticity plots, the shear layer structures are different between the 2 valves showing larger ones downstream of the leaflets. To evaluate the generated levels of viscous shear stresses and following the same method as for the instantaneous vorticity results, Fig. 14 shows the probability distribution of viscous shear stress (VSS) downstream of the valve with and without SH coating in the upper, lower and both shear layers as indicated in the figure inset. The magnitude of VSS obtained with SH coating spanned a range (combining both shear layers as shown in the inset of Fig. 13) going from −5.0Pa to +6.0Pa. A smaller range was obtained without SH coating going from −4.0Pa to +5.0Pa

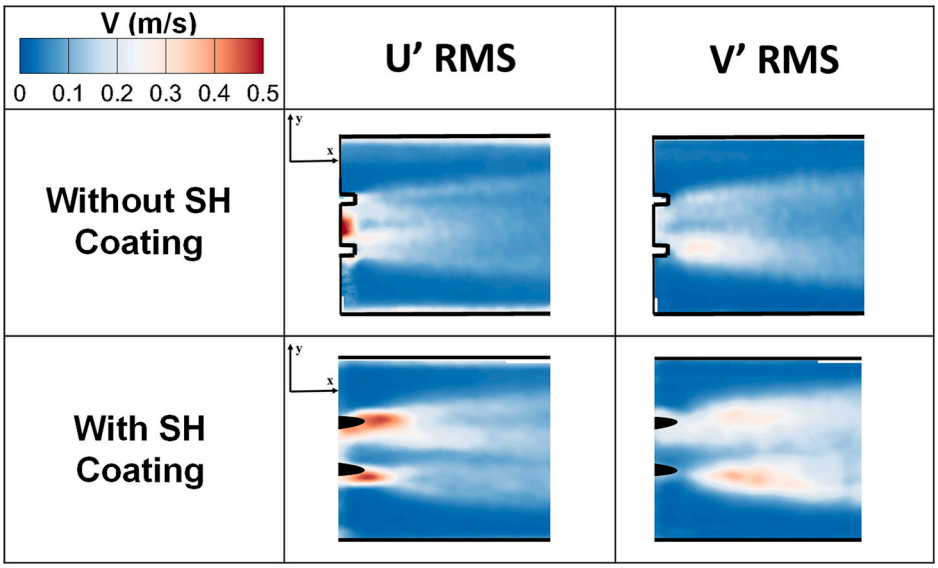

Fig. 11. Standard deviation contour plots of the random velocity fluctuations U′ and V′ for the valve models at peak systole without and with SH coating. RMS, Root mean square.

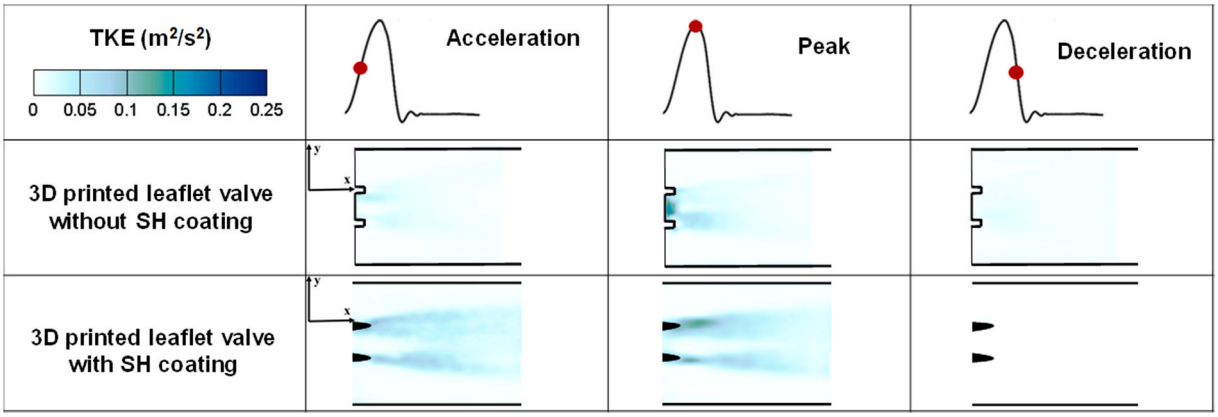

Fig. 12. Turbulent kinetic energy (TKE) at different phases in the cardiac cycle.

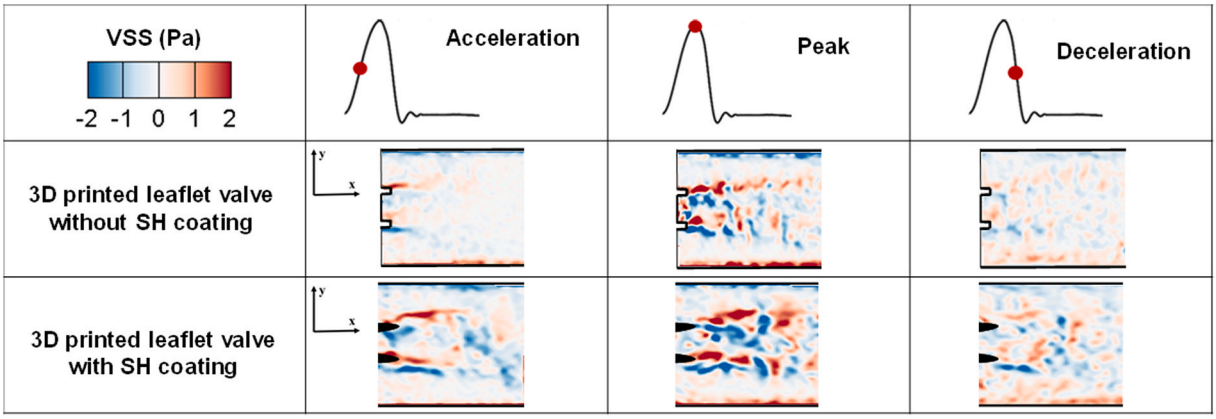

Fig. 13. Instantaneous viscous shear stress contours at different phases during the cardiac cycle.

approximately.

4. Discussion

In this study, the influence of superhydrophobicity on heart valve hemodynamics and turbulence was evaluated. With thrombus formation being one of the most crucial and dangerous adverse effects that plague prosthetic heart valves whether mechanical (Roudaut et al., 2007b) (mostly), bioprosthetic and even the transcatheter valves (Chakravarty et al., 2017), novel materials are required for investigation to minimize

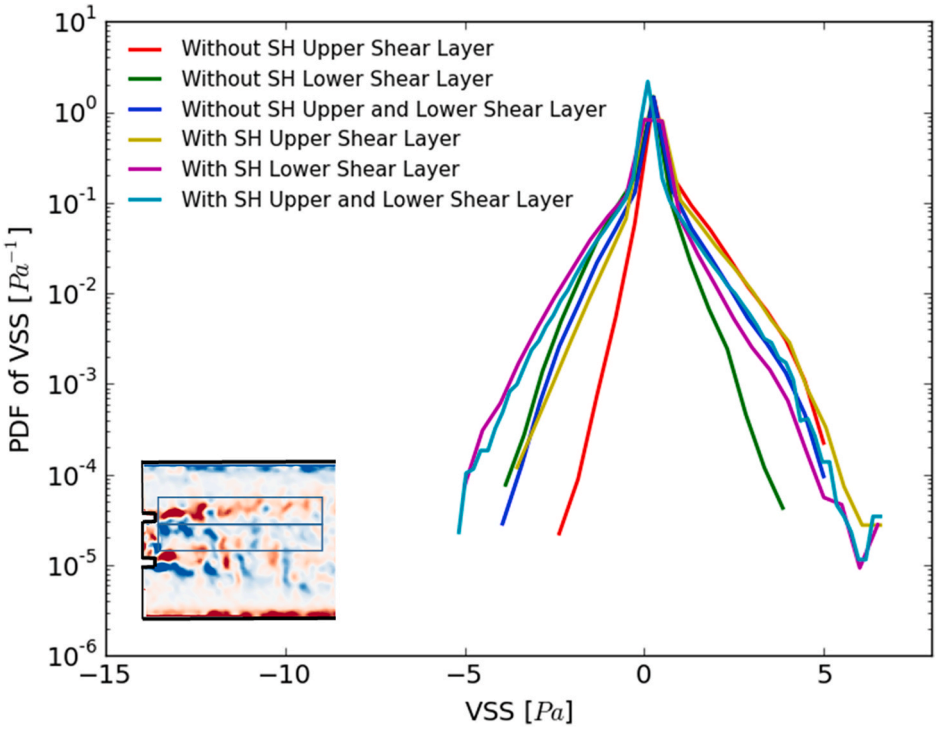

Fig. 14. Probability distribution of instantaneous viscous shear stress magnitudes of the valves with and without SH coating throughout the cardiac cycle.

if not eliminate the occurrence of thrombosis.

The mechanical heart valve by itself is non-porous. However, the SH coating is rough or textured (Fig. 2a). The air within the roughness or the texture remains trapped even after a liquid (e.g., water or our blood analogue) comes in contact with it. In other words, the contacting liquid partly levitates on a cushion of air (similar to a puck on an air hockey table levitating on a cushion of air). Such a state, with air trapped in the solid texture beneath the contact liquid, is called Cassie-Baxter state (Cassie and SJTotFs, 1944). This Cassie-Baxter state, with the trapped air, is the primary reason for extreme repellency of a SH coating to water and our blood analogue. This phenomenon is well-established and well-studied for many decades (Kota et al., 2012, 2014). Without the trapped air, the water and our blood analogue will not be able to display very low adhesion (evidenced by the very high contact angles and low roll off angles).

Due to the presence of trapped air in contact with the liquid (e.g., blood analogue), indeed there is dissolution of air from the surface, until an equilibrium is established between the trapped air and the dissolved air, determined the dissolution limit, according to Henry's law (Japas and Sengers, 1989). Prior work has shown that for very small (i.e., sub-micron) inter-feature spacings, the trapped air can exhibit infinite lifetime thereby preventing any change in performance (i.e., liquid repellency) (Xu et al., 2014; Jones et al., 2015). In our experiments, the valves retained their superhydrophobic characteristics even after experiments were finished.

In this study we saw that from a hemodynamics perspective, applying SH coating led to an increase in pressure gradient and a decrease in effective orifice area consequently. However, in both cases, the differences were not clinically important (less than 1 mmHg for pressure gradient). In what follows we discuss the mechanisms we believe are important to understand the observed increases in turbulence and how future studies may be useful to employ flow control approaches:

SH surfaces influence the flow adjacent to the coating through altering the velocity boundary condition as well as through the roughness (from the coating). While the shear-free interface (from free slip condition) is one factor that could attenuate turbulence, the surface roughness is another that works in the opposite direction (Abu Rowin and Ghaemi, 2019). Several studies demonstrated the feasibility of drag reduction in turbulent flows over superhydrophobic surfaces (Daniello et al., 2009; Martell et al., 2009). However, the surface drag reduction was sensitive to Reynolds number and to the method the superhydrophobicity is fabricated (texture, roughness and geometry among others). With prosthetic mechanical valves, details on the nature of the boundary layers on the leaflets are not yet well understood or characterized and future studies are necessary to better understand the flow and significance of the boundary layer over the mechanical heart valve leaflets (Bluestein et al., 2000; Peacock, 1990). Important changes in velocity profiles and Reynolds shear stresses are observed for a variety of geometries (Martell et al., 2009). With increasing Reynolds number and the consequent decrease of the viscous sublayer, the impact of the superhydrophobic surface on the velocity profile within the viscous sublayer becomes more important. This impact is translated into a reduction of momentum transfer from the fluid to the surface wall leading to decreasing the turbulence intensity and increasing drag reduction (Daniello et al., 2009; Gose et al., 2018). Therefore, the higher the Reynolds number the larger the expected drag reduction is. This is true if the surface considered is a superhydrophobic microridge surface, which highlights the importance of superhydrophobicity geometry and texture. Park et al. (2014) performed drag reduction studies in turbulent flow using superhydrophobic surfaces including ridges and reported no drag reduction to 70% drag reduction. Jung and Bhushan (2010) performed another study only using posts and found that drag reduction could range from 0 to 30%. When using random surface textures (that could be spray), Bidkar et al. (2014) found that there could be drag increase of −13% to drag reduction of 30%. Aljallis et al. (2013) found that there could also be drag increase (−30%) and drag decrease (30%).

In our study the fact that the SH surface is at an angle to the incoming flow in addition to the highly time dependent flow conditions makes the dynamics more complex. For the bileaflet mechanical valve, the pressure drop is not only due to the skin drag but also significantly more from the form drag from the flow separation and distal turbulence. This study clearly showed that applying the SH coating led to an increase in turbulent stresses and transvalvular pressure gradients compared to the

case where no coating was applied. Given that the surface texture utilized in our study falls under the "random" category (Fig. 2), along with not being smooth, drag reduction does not necessarily occur. In addition to that, while slip in the direction of the flow can result in drag reduction, studies have shown that slip in the spanwise direction can lead to an upsurge in the intensity of turbulent structures, causing a drag increase (Gose et al., 2018; Min and Kim, 2004; Woolford et al., 2009; Jelly et al., 2014), which may also explain the results obtained in this study. The presence of SH coating may also be believed to drive the instantaneous cross-flow from the near-wall regions towards the center of the flow plane leading to more secondary flow (Vidal et al., 2018) compared to the case where no SH coating was employed. During deceleration phase with the addition of backflow events, the flow becomes more polarized leading to more upsurge in turbulent structures and eddies (Vinuesa et al., 2017). These however need future experimental studies to confirm.

In addition to RSS results, the viscous shear stress results in this study were higher with the SH coating compared to the valve leaflets without any coating. As with SH coating the interface velocity gradients are smaller, the viscous stresses are therefore smaller at the contact areas compared with the surfaces without any SH coating (Abu Rowin and Ghaemi, 2019) within the measurement domain.

However, the shed vortices downstream of the bileaflet leaflets make room for significantly high vorticity and viscous shear stresses because of the existence of high streamwise velocity at the distal leaflet tip. This explain the higher values of vorticity, and viscous stresses obtained with SH coating. Vortex shedding is directly relevant to flow past mechanical heart valves (Bluestein et al., 2000). This observation seems to have been enhanced with SH coating leading to higher RSS and VSS. The SH coating interaction with the flow has caused the shear layers to roll-up into discrete vortices. A recent publication by Zolfaghari & Obrist (Zolfaghari and DJPrf, 2019) described an instability close to the leading edge of the leaflets (impinging leading edge vortex instability). They showed that this instability interacts later with a Burgers vortex sheet from the trailing edge of the leaflets. Figs. 5 and 13 suggest that the impinging leading-edge vortex instability may be suppressed by the coating (less fluctuations and shear stresses between the leaflets with coating), while the Burgers vortex sheet at the trailing edge is still there.

To translate these findings to clinical applications, it is important to understand the significance of the results in terms of how they relate to blood damage and thrombus formation in mechanical heart valves. Platelet activation is the first step in the process towards thrombus formation (Bark and Ku, 2013). Going with Hellum's thresholds for VSS to be 10.5 Pa (Hellums, 1993) and RSS thresholds by Liu et al. (2000), Hung et al. (1976), our study shows that despite SH coating platelet activation may be continued to be expected. However, given the beneficial surface properties of the SH coating clinical implementation may require combining the SH coating with flow control strategies to reduce turbulence. Reduction of turbulence with mechanical aortic valves was successfully achieved through the implementation of particular configurations of vortex generators on the leaflets (Hatoum and Dasi, 2019). Ongoing work combining both SH coating and vortex generators is currently underway.

4.1. Limitations

Drag reduction in most of the studies was expressed in terms of drag reduction percentage (a ratio of different skin frictions, a ratio of pressure differences, a ratio of shear-free area and dimensionless channel depth or radius) (Rothstein, 2010). While drag was not directly computed in this work, the reference to drag measurements stems from the fact that any hemodynamic study performed on superhydrophobic surfaces reported and discussed drag solely and our discussion mentions drag as an evidence in the upsurge in the intensity of turbulent structures. Currently, the effect of SH surfaces in reducing drag is still ongoing and a lot of questions need to be addressed.

The water-glycerine mixture utilized as blood analogue in this study, with density (~1060 kg/m^3) and viscosity (~3.5 cSt) similar to whole blood. Consequently, the inertial and viscous interactions between our blood analogue and the superhydrophobic (SH) coating is anticipated to be similar to whole blood and the SH coating (Movafaghi et al., 2017, 2019). However, the surface tension of the blood analogue was measured to be 68 ± 0.5 mN/m. This is slightly higher than the surface tension of whole blood (~56 mN/m). Consequently, the capillary interactions between our blood analogue and the SH coating are anticipated to be slightly different from whole blood and the SH coating. More specifically, our blood analogue displays very low adhesion on the SH coating with an advancing contact angle, receding contact angle and roll off angle of 155°, 150° and 3° (with 20 μL droplet), respectively. In contrast, we anticipate whole blood to display slightly higher adhesion on the SH coating with lower contact angles and higher roll off angles.

While it's at the cellular scale that thrombosis and hemolysis are initiated, the viscous stresses do not directly describe the microscopic flow field experienced by red blood cells and platelets. However, the spatial and temporal resolutions of the experiments performed in this study are sufficient to capture scales below the Taylor scale (estimated from a bench mark paper previously published (Morshed et al., 2014) based on the longitudinal 2-point correlation function and regarded as the conventional cut-off length scale separating the dissipative regime and the scales where inertia is more dominant (non-dissipative scales)) – if not all the way to the Kolmogorov scales (Morshed et al., 2014). Based on this, the flow structure is reasonably smooth below the Taylor scale and the estimates of VSS are reasonable. Nevertheless, our study comprehensively compares the large-scale features of the flow including turbulence. Any changes in the small-scale will (in theory) mirror the changes in the large scale.

5. Conclusion

This study evaluated the hemodynamics downstream a mechanical aortic valve with and without superhydrophobic coating in the context of assessing the potential of superhydrophobicity in reducing blood damage risk. The SH coating utilized in this study was a spray-based coating of random texture to achieve superhydrophobicity. While many studies in literature as previously discussed showed that there is potential for drag reduction, this study showed that the SH coating did not necessarily reduce pressure gradients or downstream turbulence. Future studies are needed to combine the beneficial surface characteristics of SH coatings with flow control strategies.

Declaration of competing interest

The authors declare that they have no known competing financial interests or personal relationships that could have appeared to influence the work reported in this paper.

Acknowledgment

The research done was partly supported by National Institutes of Health (NIH) under Award Number R01HL135505, R21HL139208, the American Heart Association (AHA) under Award Number 19POST34380804 and and the National Science Foundation (NSF) under Award Number 1751628.

References

Abu Rowin, W., Ghaemi, S., 2019. Streamwise and spanwise slip over a superhydrophobic surface. J. Fluid Mech. 870, 1127–1157.

Aljallis, E., Sarshar, M.A., Datla, R., Sikka, V., Jones, A., Choi, C.H., 2013. Experimental study of skin friction drag reduction on superhydrophobic flat plates in high Reynolds number boundary layer flow. Phys. Fluids 25, 14.

Bark, D.L., Ku, D.N., 2013. Platelet transport rates and binding kinetics at high shear over a thrombus. Biophys. J. 105, 502–511.

Bark, D.L., Vahabi, H., Bui, H., Movafaghi, S., Moore, B., Kota, A.K., Popat, K., Dasi, L.P., 2017. Hemodynamic performance and thrombogenic properties of a superhydrophobic bileaflet mechanical heart valve. Ann. Biomed. Eng. 45, 452–463.
Baudet, E.M., Oca, C., Roques, X., Laborde, M., Hafez, A., Collot, M., Ghidoni, I., 1985. A 5 1/2 year experience with the St. Jude Medical cardiac valve prosthesis. Early and late results of 737 valve replacements in 671 patients. J. Thorac. Cardiovasc. Surg. 90, 137–144.
Bezuidenhout, D., Zilla, P., 2013. Flexible Leaflet Polymeric Heart Valves Cardiovascular and Cardiac Therapeutic Devices. Springer, pp. 93–129.
Bidkar, R.A., Leblanc, L., Kulkarni, A.J., Bahadur, V., Ceccio, S.L., Perlin, M., 2014. Skin-friction drag reduction in the turbulent regime using random-textured hydrophobic surfaces. Phys. Fluids 26, 18.
Bluestein, D., Rambod, E., Gharib, M., 2000. Vortex shedding as a mechanism for free emboli formation in mechanical heart valves. J. Biomech. Eng. 122, 125–134.
Cassie, A., SJTotFs, Baxter, 1944. Weettabil. Porous Surf. 40, 546–551.
Chakravarty, T., Sondergaard, L., Friedman, J., De Backer, O., Berman, D., Kofoed, K.F., Jilaihawi, H., Shiota, T., Abramowitz, Y., Jorgensen, T.H., Rami, T., Israr, S., Fontana, G., de Knegt, M., Fuchs, A., Lyden, P., Trento, A., Bhatt, D.L., Leon, M.B., Makkar, R.R., Investigator, R., Investigator, S., 2017. Subclinical leaflet thrombosis in surgical and transcatheter bioprosthetic aortic valves: an observational study. Lancet 389, 2383–2392.
Chang, B.-C., Lim, S.H., Kim, D.K., Seo, J.Y., Cho, S.Y., Shim, W.H., Chung, N., Kim, S.S., Cho, B.K., 2001. Long-term results with St. Jude Medical and CarboMedics prosthetic heart valves. J. Heart Valve Dis. 10, 185–194 discussion195.
Dale, J., Myhre, E., 1978. Intravascular hemolysis in the late course of aortic valve replacement. Relation to valve type, size, and function. Am. Heart J. 96, 24–30.
Daniello, R.J., Waterhouse, N.E., Rothstein, J.P., 2009. Drag reduction in turbulent flows over superhydrophobic surfaces. Phys. Fluids 21, 9.
Ge, L., Dasi, L.P., Sotiropoulos, F., Yoganathan, A.P., 2008. Characterization of hemodynamic forces induced by mechanical heart valves: Reynolds vs. viscous stresses. Ann. Biomed. Eng. 36, 276–297.
Gose, J.W., Golovin, K., Boban, M., Mabry, J.M., Tuteja, A., Perlin, M., Ceccio, S.L., 2018. Characterization of superhydrophobic surfaces for drag reduction in turbulent flow. J. Fluid Mech. 845, 560–580.
Grigioni, M., Daniele, C., D'Avenio, G., Barbaro, V., 1999. A discussion on the threshold limit for hemolysis related to Reynolds shear stress. J. Biomech. 32, 1107–1112.
Gunning, P.S., Saikrishnan, N., McNamara, L.M., Yoganathan, A.P., 2014. An in vitro evaluation of the impact of eccentric deployment on transcatheter aortic valve hemodynamics. Ann. Biomed. Eng. 42, 1195–1206.
Hatoum, H., Dasi, L.P., 2019. Reduction of pressure gradient and turbulence using vortex generators in prosthetic heart valves. Ann. Biomed. Eng. 47, 85–96.
Hatoum, H., Gooden, S., Heitkemper, M., Blum, K.M., Zakko, J., Bocks, M., Yi, T., Wu, Y.-L., Wang, Y., Breuer, CKJAoBE., 2020. Fetal Transcatheter Trileaflet Heart Valve Hemodynamics: Implications of Scaling on Valve Mechanics and Turbulence, pp. 1–11.
Hatoum, H., Lilly, S., Maureira, P., Crestanello, J., L.P., Dasi, surgery, c, 2019a. The Hemodynamics of Transcatheter Aortic Valves in Transcatheter Aortic Valves.
Hatoum, H., Maureira, P., Dasi, L.P., 2019b. A turbulence in vitro assessment of On-X and St Jude Medical prostheses. J. Thorac. Cardiovasc. Surg. 47 (1), 85–96.
Hatoum, H., Maureira, P., Lilly, S., Dasi, L.P., 2019c. Impact of leaflet laceration on transcatheter aortic valve-in-valve washout: BASILICA to solve neosinus and sinus stasis. JACC Cardiovasc. Interv. 12 (13), 1229–1237.
Hellums, J.D., 1993. Whitaker Lecture: biorheology in thrombosis research. Ann. Biomed. Eng. 22, 445–455, 1994.
Horbett, T.A., Brash, J.L., 1987. Proteins at interfaces: current issues and future prospects. Proteins Interfaces Physicochem. Biochem. Studies 343, 1–33.
Hung, T., Hochmuth, R., Joist, J., Sutera, S., 1976. Shear-induced aggregation and lysis of platelets. Am. Soc. Artif. Intern. Organs J. 22, 285–290.
Jaffer, I., Fredenburgh, J., Hirsh, J., Weitz, J., 2015. Medical device-induced thrombosis: what causes it and how can we prevent it? J. Thromb. Haemostasis 13, S72–S81.
Japas, M., Sengers, JLJAj, 1989. Gas solubility and Henry's law near the solvent's critical point, 35, 705–713.
Jelly, T.O., Jung, S.Y., Zaki, T.A., 2014. Turbulence and skin friction modification in channel flow with streamwise-aligned superhydrophobic surface texture. Phys. Fluids 26.
Jones, P.R., Hao, X., Cruz-Chu, E.R., Rykaczewski, K., Nandy, K., Schutzius, T.M., Varanasi, K.K., Megaridis, C.M., Walther, J.H., PJSr, Koumoutsakos, 2015. Sustain. Dry Surf. Water. 5, 12311.
Jung, Y.C., Bhushan, B., 2010. Biomimetic structures for fluid drag reduction in laminar and turbulent flows. J. Phys. Condes. Matter. 22, 9.
Kameneva, M.V., Burgreen, G.W., Kono, K., Repko, B., Antaki, J.F., Umezu, M., 2004. Effects of turbulent stresses upon mechanical hemolysis: experimental and computational analysis. Am. Soc. Artif. Intern. Organs J. 50, 418–423.
Khorasani, M., Mirzadeh, H., 2004. In vitro blood compatibility of modified PDMS surfaces as superhydrophobic and superhydrophilic materials. J. Appl. Polym. Sci. 91, 2042–2047.
Kota, A.K., Li, Y., Mabry, J.M., Tuteja, AJAm, 2012. Hierarchically Structured Superoleophobic Surfaces with Ultralow Contact Angle Hysteresis, vol. 24, pp. 5838–5843.
Kota, A.K., Kwon, G., Tuteja, A.J.N.A.M., 2014. The Design and Applications of Superomniphobic Surfaces, vol. 6 e109-e109.
Liu, J., Lu, P., Chu, S., 2000. Turbulence characteristics downstream of bileaflet aortic valve prostheses. J. Biomech. Eng. 122, 118–124.
Martell, M.B., Perot, J.B., Rothstein, J.P., 2009. Direct numerical simulations of turbulent flows over superhydrophobic surfaces. J. Fluid Mech. 620, 31–41.
Min, T.G., Kim, J., 2004. Effects of hydrophobic surface on skin-friction drag. Phys. Fluids 16, L55–L58.
Morshed, K.N., Bark Jr., D., Forleo, M., LPJPo, Dasi, 2014. Theory to Predict Shear Stress on Cells in Turbulent Blood Flow, vol. 9.
Movafaghi, S., Leszczak, V., Wang, W., Sorkin, J.A., Dasi, L.P., Popat, K.C., AKJAhm, Kota, 2017. Hemocompat. Superhemoph. Titania. Surf. 6, 1600717.
Movafaghi, S., Wang, W., Bark, D.L., Dasi, L.P., Popat, K.C., 2019. Hemocompatibility of super-repellent surfaces: current and future. Mater. Horiz. 6 (8), 1596–1610.
Park, H., Sun, G.Y., Kim, C.J., 2014. Superhydrophobic turbulent drag reduction as a function of surface grating parameters. J. Fluid Mech. 747, 722–734.
Peacock, JAJCr, 1990. An in Vitro Study of the Onset of Turbulence in the Sinus of Valsalva, vol. 67, pp. 448–460.
Rajput, F.A., Zeltser, R., 2019. Aortic Valve Replacement *StatPearls [Internet]*. StatPearls Publishing.
Rothstein, J.P., 2010. Slip on superhydrophobic surfaces. Annu. Rev. Fluid Mech. Palo. Alto. Annu. Rev. (42), 89–109.
Roudaut, R., Serri, K., Lafitte, S., 2007a. Thrombosis of prosthetic heart valves: diagnosis and therapeutic considerations. Heart 93, 137–142.
Roudaut, R., Serri, K., Lafitte, S., 2007b. Valve disease - thrombosis of prosthetic heart valves: diagnosis and therapeutic considerations. Heart 93, 137–142.
Shapira, Y., Vaturi, M., Sagie, A., 2009. Hemolysis associated with prosthetic heart valves: a review. Cardiol. Rev. 17, 121–124.
Stein, P.D., Sabbah, H.N., 1974. Measured turbulence and its effect on thrombus formation. Circ. Res. 35, 608–614.
Sultan, I., Bianco, V., Gleason, T.G., Aranda-Michel, E., Navid, F., Kilic, A., 2019. Clinical outcomes and hospital readmission rates in mechanical vs bioprosthetic mitral valves. J. Card. Surg. 34 (7), 555–562.
Sun, T., Tan, H., Han, D., Fu, Q., Jiang, L., 2005. No platelet can adhere—largely improved blood compatibility on nanostructured superhydrophobic surfaces. Small 1, 959–963.
Vidal, A., Nagib, H., Schlatter, P., RJJoFM, Vinuesa, 2018. Secondary Flow in Spanwise-Periodic In-phase Sinusoidal Channels, vol. 851, pp. 288–316.
Vinuesa, R., Örlü, R., PJJoT, Schlatter, 2017. Characterisation of Backflow Events over a Wing Section, vol. 18, pp. 170–185.
Vongpatanasin, W., Hillis, L.D., Lange, R.A., 1996. Prosthetic heart valves. N. Engl. J. Med. 335, 407–416.
Voronov, R.S., Papavassiliou, D.V., Lee, L.L., 2008. Review of fluid slip over superhydrophobic surfaces and its dependence on the contact angle. Ind. Eng. Chem. Res. 47, 2455–2477.
Woolford, B., Prince, J., Maynes, D., Webb, B.W., 2009. Particle image velocimetry characterization of turbulent channel flow with rib patterned superhydrophobic walls. Phys. Fluids 21.
Xu, M., Sun, G., Kim, C.J., 2014. Infinite lifetime of underwater superhydrophobic states, 113, 136103.
Zolfaghari, H., DJPrf, Obrist, 2019. Absolute instability of impinging leading edge vortices in a submodel of a bileaflet mechanical heart valve, 4, 123901.